HHS Public Access

Author manuscript

J Mol Biol. Author manuscript; available in PMC 2026 February 05.

Published in final edited form as:

J Mol Biol. 2025 December 15; 437(24): 169490. doi:10.1016/j.jmb.2025.169490.

Biochemical and Structural Analyses of the Tardigrade DNA-Damage Suppressor Protein, Dsup

Tyler J. Woodward,

M. Todd Washington

Department of Biochemistry and Molecular Biology, University of Iowa College of Medicine, Iowa City, IA 52242-1109, United States

Abstract

Tardigrades are extremophiles that withstand harsh environments through unique molecular strategies. One such strategy involves Damage Suppressor (Dsup), a protein shown to protect cells from radiation-induced DNA damage. Little is known about the biochemical and structural characteristics of Dsup that lead to DNA protection. To gain insight into the mechanism of DNA protection by Dsup, we examined its fundamental biochemical and structural properties using mass photometry, biolayer interferometry, small-angle X-ray scattering, and microfluidic modulation spectroscopy. We found that Dsup is largely intrinsically disordered and binds DNA with high affinity via a multi-valent interface. This interaction induced conformational changes in both Dsup and the DNA, suggesting a potential structural mechanism of its DNA protection ability. We propose that Dsup alters DNA structure, possibly by partially unwinding it, to reduce its susceptibility to damage. These findings offer new insights into how a disordered protein such as Dsup functions as radioprotectants in extreme environments.

Keywords

DNA repair; genome stability; intrinsically disorder proteins; protein-DNA interactions

Introduction

Life has evolved a variety of mechanisms to cope with extreme environmental conditions. These mechanisms allow extremophiles, such as archaea and bacteria, to thrive in boiling hydrothermal vents and other organisms to survive arctic conditions. Tardigrades, which are microscopic invertebrates found in a wide range of environments, are one such extremophile

Correspondence to M. Todd Washington: Department of Biochemistry and Molecular Biology, 4-403 Bowen Science Building, University of Iowa, Iowa City, IA 52242-1109, United States. todd-washington@uiowa.edu *(M.T. Washington).*

CRediT authorship contribution statement

Tyler J. Woodward: Writing – review & editing, Writing – original draft, Visualization, Validation, Methodology, Investigation, Formal analysis, Data curation, Conceptualization. **M. Todd Washington:** Writing – review & editing, Writing – original draft, Visualization, Validation, Supervision, Methodology, Investigation, Funding acquisition, Formal analysis, Conceptualization.

DECLARATION OF COMPETING INTEREST

The authors declare that they have no known competing financial interests or personal relationships that could have appeared to influence the work reported in this paper.

[1–3]. Tardigrades can survive extremes in temperatures from near absolute zero to over 100 °C and immense pressures from zero to 1,200 atm [1–7]. Remarkably, tardigrades are also highly resistant to radiation, enduring doses as high as 4,000– 5,000 Gy [1,4–7] – approximately one thousand times more radiation than mammals can endure. One of the key adaptations of tardigrades is anhydrobiosis, a process in which nearly all intracellular water is removed, allowing survival in extreme environments [8]. While early studies suggested that desiccation alone was sufficient for radiation resistance, subsequent work has shown that some tardigrade species – particularly *Ramazzottius varieornatus* – are highly radiotolerant even in the hydrated state, suggesting the presence of other protective mechanisms [5–10]. This finding has sparked research into the cellular mechanisms that tardigrades use to protect against radiation.

Sequencing the R. varieornatus genome revealed the presence of a tardigrade-specific gene, which is essential for its extreme radiotolerance [9]. This gene encodes a protein that localizes to the nucleus and is predicted to be intrinsically disordered [9]. It was hypothesized that the extended and disordered nature of the protein is vital to its protective function. Thus, this protein was called Damage Suppressor (Dsup). Dsup possesses minimal homology to known proteins [9–11], and it binds to both free DNA and nucleosomes [12–14].

Expression of Dsup in mammalian cells protects them against DNA damage induced by ionizing and ultraviolet radiation [9–13,15]. For example, HEK-293T cells expressing Dsup showed nearly 50% less DNA damage upon exposure to 10 Gy of X-ray radiation compared to cells lacking Dsup [9]. There is also significantly reduced DNA damage caused by hydrogen peroxide, a reactive oxygen species generated by ionizing radiation [9,11]. Furthermore, exposure to UV C radiation led to fewer cyclobutane pyrimidine dimers for cells expressing Dsup compared to cells lacking Dsup [15]. Despite these advances in our understanding of the function of Dsup, its precise mechanism for radiotolerance remains unclear. This is largely because many key biochemical properties of Dsup remain poorly understood. For example, there are no studies to our knowledge describing the oligomeric state, optimal DNA-ligand length, or structure–function relationships of Dsup.

To gain insight into the mechanism of DNA protection by Dsup, we examined its fundamental biochemical and structural properties using a combination of experimental and computational techniques. We found that Dsup predominantly exists as a monomer in solution and that it is largely disordered in the absence of DNA. In addition, Dsup binds both single-stranded and double-stranded DNA with high affinity. The affinity decreased for DNA ligands shorter than 30 bp, suggesting that the optimal length for DNA binding is approximately 30 or more bp. In addition, we showed that the central region of Dsup (residues 180–270) appears to be critical for achieving high-affinity DNA binding. Importantly, we found that Dsup becomes more structured when binding to DNA and this reduces the amount of base-pairing in the DNA. We propose that specific interactions with key Dsup residues alter the structure of the DNA and reduce the likelihood of damage.

Materials and Methods

Protein expression and purification

Full-length Dsup (residues 1–445) was cloned into pET21b with a N-terminal 6xHis tag and C-terminal FLAG tag (Supplemental Figure S1). This plasmid (pKW805) was transformed into BL21 (DE3) pLysS, and the protein was over-expressed by growing cells at 18 °C overnight with 1 mM IPTG. Cells were lysed using a C3-Avestin Emulsiflex homogenizer in the presence of DNase, PMSF, and a Roche cOmplete Protease Inhibitor Cocktail. The protein was purified using a series of affinity chromatography and size-exclusion chromatography steps. All buffers used contain 150 mM HEPES, pH 7.6, 150 mM sodium chloride (unless specified otherwise), and 10 mM beta-mercaptoethanol. The cell lysate was cleared by centrifugation at 16,000 rpm for 1 h at 4 °C. The cleared lysate was loaded onto a 5 mL HisTrap HP Ni Sepharose HP column (Cytiva) and eluted using a linear gradient of 100 mM–1.5 M imidazole. Next, fractions were combined and loaded onto a 5 mL HiTrap Heparin Sepharose HP column (Cytiva). Proteins were eluted using a linear gradient of 100 mM–1.5 M sodium chloride. Finally, fractions were combined and loaded onto a HiLoad Superdex S200 size-exclusion chromatography (Cytiva). Size-exclusion utilized an isocratic buffer containing 25 mM arginine, 25 mM glutamic acid, and 10% glycerol. The purity of the protein was verified using SDS PAGE. Afterwards, the protein was flash frozen in liquid N_2 and stored at −80 °C.

Additionally, several truncated forms of Dsup were over-expressed and purified as described above using plasmids pKW806 (residues 90–445), pKW807 (residues 180–445), pKW808 (residues 270–445), pKW809 (residues 355–445), and pKW810 (residues 1–355).

Oligonucleotides

All oligonucleotides were purchased from Integrated DNA Technologies (IDT). Double-stranded DNA (dsDNA) substrates of various lengths and with and without specific types of DNA damage were prepared for biolayer interferometry (BLI) and fluorescence assays. For BLI experiments, four non-damaged duplex DNA ligands of increasing length were used: a 20-mer, 30-mer, 40-mer, and 75-mer (Supplemental Table S1). The 20-mer duplex was generated by annealing oligonucleotides 01 and 02; the 30-mer from 03 and 04; the 40-mer from 05 and 06; and the 75-mer from 07 and 08. Additional dsDNA substrates containing different types of DNA damage were also prepared for BLI analysis. These included substrates with an 8-oxoguanine lesion (05 and 09), an apurinic (AP) site (05 and 10), and a single-nucleotide gap (05, 11, and 12). A separate DNA substrate containing 2-aminopurine (2-AP) was prepared for fluorescence spectroscopy experiments to monitor protein-induced conformational changes in DNA. This substrate was generated by annealing oligonucleotides 04 and 13. All duplexes were formed by mixing complementary oligonucleotides at 10 μM each in annealing buffer (10 mM Tris–HCl, pH 7.5, 50 mM NaCl, 1 mM EDTA). The mixtures were heated to 95 °C for 5 min and then slowly cooled to room temperature over several hours to allow complete annealing.

Mass photometry

A TwoMP Mass Photometer (Refeyn) was used to analyze the oligomeric state of Dsup. The protein was serially diluted in filtered PBS buffer to a final concentration of 80 nM, which was further diluted 4-fold to 20 nM on the instrument stage. The cover slides were High Precision Deckgläser No. 1.5H, 24 × 50 mm rectangle with a 170 ± 5 μm thickness. Sample were incubated at 22 °C for several minutes prior to the experiment. Detection and quantification were processed using the DiscoverMP software (Refeyn) as previously reported [16].

Small-angle X-ray scattering

Experimental small-angle X-ray scattering (SAXS) data were collected at the BioSAXS beamline at Oak Ridge National Laboratory. X-ray scattering was measured at a concentration of 0.05 mg/mL in buffer containing 50 mM HEPES, pH 7.7, 150 mM NaCl, 10 mM β-mercaptoethanol, 25 mM L-glutamic acid, and 25 mM L-arginine. A buffer only control was used to subtract the baseline scattering. Finally, scattering data were processed using the RAW software suite [17]. Structural parameters including the radius of gyration (R_g) and the maximum particle dimension (D_{max}) were obtained from the data using GNOM [18].

Brownian dynamics simulations

To examine the conformational dynamics of Dsup, we carried out coarse-grained Brownian dynamics (BD) simulations. An initial structural model of Dsup was produced using AlphaFold 3 [19]. This initial model, which was almost entirely disordered, was coarse-grained as described previously [20–22]. Briefly, each residue in the initial model was replaced by one to four pseudo-atoms (coarse-grained beads), and ionizable groups were assigned a partial charge to reflect a pH equal to 8.0. The simulations were carried out using the *uiowa_BD* code as described previously [23–25]. Briefly, the time step for the simulations was 125 fs with a PDB file produced every 1 ns. Simulations were run in triplicate for a total of 10 μs per replicate with a snapshot (PDB file) generated every 1 ns to generate final ensembles containing 10,000 structures each (30,000 structures total). For each structure in the ensemble, theoretical SAXS profiles were generated using the PDB2SAS tool from the ATSAS suite run through the RAW software interface [17]. This allowed us to plot the R_g and D_{max} as a function of time and to generate the R_g and D_{max} of the entire ensemble.

Biolayer interferometry

Biolayer interferometry (BLI) experiments were performed on an Octet RED96 instrument (ForteBio) at 25 °C using a 5-step protocol: equilibration, loading, baseline, association, and dissociation as described previously [26]. Briefly, Dsup protein was prepared in a BLI buffer containing 20 mM Tris, pH 7.5, 100 mM NaCl, 1 mM EDTA, and 0.05% Tween-20. Streptavidin biosensors were pre-soaked in buffer for at least 30 min before use. The biotinylated DNA ligands were loaded onto the sensors prior to association with Dsup. Titrations with seven Dsup concentrations were carried out at a fixed DNA concentration, with one sample serving as a reference without Dsup. Control experiments were performed

in which no DNA was loaded onto the sensors prior to analyte association. The control experiments with no DNA and the no-Dsup sample were applied as a double reference when analyzing the total binding data. Data were processed with the Data Analysis software (ForteBio) and analyzed using Prism 10 (GraphPad).

Microfluidic modulation spectroscopy

Infrared spectra of full-length Dsup (residues 1–445), a 40-mer double-stranded DNA ligand, and the Dsup–DNA complex were collected using the Aurora TX Microfluidic Modulation Spectroscopy system (RedShiftBio) [27,28]. Dsup–DNA complexes were prepared by incubating the full-length protein with annealed 40-mer dsDNA at a 1:1 M ratio for 30 min at room temperature. Prior to analysis, all samples were buffer-exchanged into a buffer containing 50 mM HEPES (pH 7.7), 150 mM NaCl, 10 mM β-mercaptoethanol, 25 mM L-glutamic acid, 25 mM L-arginine, and 7.5% glycerol using Amicon Ultra centrifugal filters (Millipore).

Spectra were recorded at 25 °C in triplicate with real-time buffer reference subtraction against the matching buffer at a backing pressure between 17 and 18 psi with an average flow rate of 1 μL/s. Each measurement captured the full amide I band (1588–1765 cm^{-1}) at 1 cm^{-1} resolution. The inverse second derivative of the absorbance spectra was calculated to identify changes in secondary structure. Data normalization, baseline-correction, and spectral subtraction were performed using the delta analytics software (RedShiftBio) [27,28].

Fluorescence spectroscopy

Fluorescence spectroscopy experiments utilized a Cary Eclipse Fluorescence Spectrometer. The excitation wavelength was set to 303 nm, while the emission wavelength was set to 370 nm. The excitation and emission slits were both set to 10 nm. Using the kinetics mode, 488 μL of buffer (50 mM HEPES, pH 7.5, 150 mM NaCl) was placed into a 600 μL quartz cuvette. After zeroing for the buffer, 54 μL of DNA substrate (containing 2-aminopurine) was then added to the cuvette to reach a final concentration of 1 μM. Finally, either 60 μL of buffer or 60 μL of purified Dsup (4 μM final concentration) was added to the cuvette. The experiments were conducted in triplicate, and the fluorescence signal was normalized to the emission of the DNA substrate alone prior to the addition of buffer or protein.

Blue-Native PAGE

Blue-Native PAGE was conducted using an NativePAGE™ Novex® Bis-Tris gel system. Purified Dsup protein was diluted to five different concentrations: 0.005, 0.01, 0.025, 0.05, 0.1 mg/mL (0.1, 0.2, 0.5, 1, 2 μM). A 15-well 3–12% Invitrogen commercial native gel was used. Wells were rinsed with MilliQ water, and subsequently three-times with dark blue cathode buffer (10 mL 20× NativePAGE running buffer, 10 mL of 20× Cathode buffer, and 180 mL of MilliQ water). Anode buffer was prepared by mixing 50 mL of 20× NativePAGE running buffer with 950 mL of MilliQ water. Both cathode and anode buffers were pre-chilled to 4 °C prior to electrophoresis. The gel was loaded with 10 μL of each sample. The gel was then run at 150 V for 75 min. Finally, the gel was fixed in a 40%

methanol and 10% acetic acid solution for 30 min. The gel was then de-stained with 8% acetic acid overnight.

Results

Oligomeric state of Dsup

To determine whether Dsup exists as a monomer or as higher-order oligomeric species in solution, we examined the oligomeric state of Dsup using mass photometry (Figure 1A) [16]. We found that approximately 90% of the protein has a molecular weight of 43 ± 6 kDa, which corresponds to the mass of a monomer with its 6xHis and FLAG affinity tags (45 kDa). We also found that approximately 10% of the protein had a molecular weight of 91 ± 13 kDa, which corresponds to the mass of a dimer. This shows that at protein concentrations around 20 nM, Dsup exists predominantly as a monomer in solution with a small, but detectable amount of dimer present.

We next examine the oligomeric form of Dsup at higher protein concentrations ranging from 0.1 to 2 μM using blue-native PAGE (Figure 1B). We found that nearly all of the Dsup protein has an electrophoretic mobility consistent with a monomer. The mass photometry and blue-native PAGE results both support the notion that Dsup is primarily a monomer in solution over a wide range of protein concentrations.

Overall structure of Dsup

To better understand the overall structure of Dsup in solution, we used a small-angle X-ray scattering (SAXS) (Figure 2). First, we obtained a scattering curve showing the intensity of X-ray scattering as a function of q, the radial distance from the center of the detector (Figure 2A). From this data, we generated a Guinier plot, which showed that Dsup is not prone to aggregation. Furthermore, we generated a pairwise distribution plot ($P(r)$ plot), which showed that the radius of gyration (R_g) is 78 Å and the maximum particle dimension (D_{max}) is 290 Å (Figure 2C). These R_g and D_{max} values are significantly larger than expected for a globular protein with a mass of 45 kDa (which would be about 25 Å and 80 Å, respectively). This implies that Dsup is a highly extended and potentially intrinsically disordered protein. To verify this, we generated a Kratky plot, which indicated that Dsup is indeed predominantly disordered, as indicated by the absence of a pronounced peak and failure to return to baseline at higher scattering vectors (Figure 2D).

Conformational flexibility of Dsup

The SAXS analysis showed that Dsup is highly extended and intrinsically disordered. This implies that Dsup possesses a high degree of conformational flexibility and samples an extremely large region of conformational space. To examine the conformational flexibility of Dsup, we carried out Brownian dynamics (BD) simulations of Dsup (Figure 3). We built an initial model of Dsup using AlphaFold 3, which was almost entirely disordered. This starting model had calculated R_g and D_{max} values of 79 Å and 257 Å, respectively, which are very close to the experimentally determined R_g and D_{max} values obtained from SAXS (78 Å and 290 Å, respectively). We then ran coarse-grained BD simulations of the Dsup protein in triplicate. We obtained structural snapshots of Dsup every 1 ns over the duration of the 10

μs simulation. This generated an ensemble of 10,000 structural snapshots of Dsup for each replicate.

For each structural snapshot of Dsup, we calculated the R_g and D_{max} values and graphed them as a function of simulation time (Figure 3A, B). These values fluctuated over the course of the simulations but did not show either an upward or a downward trend indicating that the simulations reached an equilibrium point and contained many energy-equivalent conformations. In addition, we created histograms of the R_g and D_{max} values to better visualize the distribution of values (Figure 3C, D). To visualize these conformations, four sample snapshots representing the 20th, 40th, 60th, and 80th percentiles of the ensemble with respect to R_g are shown in Figure 3E. We finally determined the R_g and D_{max} values for the entire ensemble of snapshots, which were 78 Å and 290 Å, respectively. The predicted scattering curve for the full ensemble agreed with the experimental scattering curve with a χ^2 equal to 5.8. Ultimately, the full ensemble is consistent with both the mass photometry data and the SAXS analyses. Taken together, these data all show that Dsup is an intrinsically disordered protein with high conformational flexibility in solution.

DNA-binding affinity of Dsup

To determine the DNA-binding affinity of Dsup, we used biolayer interferometry (BLI). We immobilized a 30-mer double-stranded DNA molecule on the surface of the probe and added various concentrations of Dsup (0–100 nM) to the wells. We measured the response units of the association and dissociation phases as a function of time and determined the response units at equilibrium (Figure 4A). We then graphed the equilibrium response units as a function of Dsup concentration and obtained a K_d value of 3.1 ± 0.7 nM (Figure 4B, Supplemental Figure S2, Table 1). We also carried out similar experiments using a 30-mer single-stranded DNA molecule rather than a duplex molecule (Figure 4C). We found that the K_d for single-stranded DNA binding is 3.2 ± 0.8 nM (Figure 4D, Supplemental Figure S2, Table 1), which is identical to the K_d for double-stranded DNA binding.

Optimal DNA length for DNA binding

To determine the optimal DNA length of Dsup for binding double-stranded DNA, we determined the affinity of Dsup for binding double-stranded DNA molecules of various lengths (20-mer, 30-mer, 40-mer, and 75-mer) (Figure 5). The K_d values for binding the 30-mer, 40-mer, and 75-mer were nearly the same, ranging from 1.5 to 3.1 nM. By contrast, the K_d for binding the 20-mer was an order-of-magnitude greater, 30 ± 8 nM (Figure 5, Supplemental Figure S3, Table 1). These findings suggest that the optimal DNA length of Dsup for DNA binding is approximately 30 or more bp.

Regions of Dsup important for DNA binding

To determine which regions of the Dsup protein contribute to DNA binding, we overexpressed and purified the C-terminal fragment (residues 355–445), previously suggested to be necessary and sufficient for DNA binding [10–12]. We used BLI to measure and compare the DNA binding affinities of full-length Dsup and this C-terminal fragment of Dsup. Whereas full-length Dsup binds a double-stranded 40-mer DNA with a K_d of 1.5 ± 0.2 nM, the C-terminal fragment of Dsup binds much weaker with a K_d of 3,300 ± 600

nM (Figure 6A, Supplemental Figure S4, Table 2). This implies that protein-DNA contacts outside the C-terminal region of Dsup are necessary for high-affinity DNA binding. To further examine the potential importance of the C-terminal region of Dsup for DNA binding, we produced another Dsup construct (residues 1–355), which lacked the C-terminal region. The protein construct lacking the C-terminal region bound DNA with a K_d of 490 ± 10 nM, which is 330-fold weaker than the binding of full-length Dsup and 7-fold stronger than the C-terminal region of Dsup alone (Figure 6B, Supplemental Figure S4). These results show that while the C-terminal region plays a role in DNA binding, this interaction is substantially enhanced by protein-DNA contacts outside of the C-terminal region of Dsup.

To identify regions outside the C-terminal region of Dsup that are important for high-affinity DNA binding, we generated a set of nested N-terminal truncations of Dsup and examined their DNA binding affinity using BLI (Figure 7, Supplemental Figure S5, Table 2). We found that the binding affinity for the DNA decreases only slightly when the first 90 or 180 residues are deleted from the N-terminus. However, the DNA binding affinity decreases substantially, ~260-fold compared to full-length Dsup, upon deletion of the first 270 residues from the N-terminus. The binding affinity for this construct (residues 270–445) is ~9-fold greater than the C-terminal region alone. Taken together, these results imply that there are important protein-DNA contacts between residues 180 and 270 of Dsup that contribute to high-affinity DNA binding. There are additional, but less important, protein-DNA contacts between residues 270 and 355 of Dsup. This suggests a model in which Dsup binds through multivalent interactions to DNA across the entire C-terminal 60% of the protein (residues 180–445).

Damaged DNA binding by Dsup

To determine whether Dsup binds damaged DNA with higher or lower affinity, we determined the K_d for Dsup binding a 40-mer double-stranded DNA molecule with a single 8-oxoguanine (8-oxoG) lesion, which was equal to 4.3 nM (Figure 8, Supplemental Figure S6, Table 3). Similarly, the K_d for Dsup binding a 40-mer DNA with a single abasic site was equal to 3.6 nM, and the K_d for binding a DNA with a single 1-nucleotide gap was equal to 7.8 nM (Figure 8, Supplemental Figure S6, Table 3). These values are nearly identical to the K_d value for the non-damaged 40-mer DNA, which was equal to 1.5 nM. This shows that Dsup binds non-damaged and damaged DNA with approximately the same affinity.

Conformational changes in Dsup and DNA upon binding

To determine whether Dsup or the DNA changes conformation upon complex formation, we utilized infrared (IR) spectroscopy to analyze the amide I band (wavenumber 1600–1700 cm^{-1}) of Dsup, DNA, and the Dsup-DNA complex. The amide I band, which primarily arises from carbonyl stretching vibrations within the protein backbone, provides detailed information regarding secondary structural elements in proteins [29,30]. Additionally, changes within this region can reflect variations in DNA base pairing, particularly shifts in the hydrogen bonding between guanine and cytosine bases [31,32]. We first collected IR absorbance spectra for full-length Dsup and a 40-mer dsDNA ligand alone (Figure 9A, C). We then calculated the inverse 2nd derivative for both spectra (Figure 9B, D). From this plot, we can calculate the relative abundance of each secondary structure component for

Dsup alone (Supplemental Figure S7). We found that the spectra of Dsup alone agree with our analysis of Dsup structure from SAXS and BD simulations. We found that at least 52 ± 9% of Dsup is disordered. In addition, the spectra for the DNA ligand alone confirm the presence of significant base pairing.

We next collected IR absorbance spectra for a 1:1 complex of Dsup and the DNA ligand. These data were compared to a theoretical spectrum, which was the sum of the spectra for Dsup alone and the DNA alone (Figure 10A). The theoretical spectrum represents the expected result if Dsup binding to DNA does not induce conformational changes in either the protein or the DNA. Therefore, differences between the experimental spectra and theoretical spectrum represent conformational changes in the protein or DNA upon binding. Thus, we compared the inverse second derivative of both the experimental and theoretical spectra (Figure 10B). We subtracted the experimental and theoretical spectra to determine if any conformational changes occurred as a result of complex formation (Figure 10C). We observed a significant loss in signal at 1,717 cm^{-1} indicating reduced base pairing between guanine and cytosine bases in the complex compared to DNA alone. Furthermore, we observed an increase in signal at 1,655 cm^{-1}, indicating more α-helical content in the complex compared to Dsup alone. These findings show that Dsup becomes more structured, and that the DNA becomes more melted or unwound upon binding.

To provide further support for the notion that Dsup binding to DNA induces a conformational change in the DNA that leads to partial melting or unwinding, we carried out fluorescence experiments using a 30-mer double-stranded DNA molecule containing two 2-aminopurines. The fluorescence of 2-aminopurine increases substantially upon DNA melting or unwinding [33–35]. We observed a significant increase in 2-aminopurine fluorescence upon Dsup binding compared to the negative control (Figure 11). Taken together, the IR spectroscopy and 2-aminopurine fluorescence results support the notion that the DNA is partially melted or unwound when Dsup binds.

Discussion

Tardigrades can survive in extreme environments including those with high levels of radiation [1–7]. In fact, tardigrades can endure radiation doses as high as 4,000–5,000 Gy – approximately one thousand times more radiation than mammals can endure [4,7]. It was once believed that this resistance to radiation was due to the removal of nearly all intracellular water [36,37]. Recent work, however, has shown that some tardigrade species are highly radiotolerant even in the hydrated state. This suggested the presence of other protective mechanisms and led to the discovery of Dsup, a DNA-binding protein responsible for protecting the genomes of tardigrades from radiation-induced DNA damage [9]. Interestingly, expression of Dsup in human cells confers a significant amount of protection from radiation [9,15]. While it is known that Dsup localizes to the nucleus and binds both free DNA and nucleosomes, little is known about the mechanism by which Dsup protects DNA from radiation-induced damage [9,11]. Arguably, the primary reason for this lack of mechanistic knowledge arises because of a lack of understanding of the biochemical and structural properties of Dsup. The objective of the work described here is to gain new

insight into the mechanism of DNA protection by Dsup by characterizing its fundamental biochemical and structural properties.

In the present study, we showed using mass photometry and native PAGE that Dsup predominantly exists as a monomer in solution. Although some dimer was observed, there were not higher-order oligomeric species detectible under the experimental conditions. Previous studies showed that Dsup binds double-stranded DNA with moderate to high affinity, with K_d estimates in the 20–40 nM range [11]. Using BLI, we rigorously measured the binding affinity of Dsup for double-stranded DNA and found that the affinity is higher than previously estimated with a K_d equal to 3.1 nM. Surprisingly, we also made the novel discovery that Dsup binds single-stranded DNA and does so with approximately the same affinity with which it binds double-stranded DNA. Similarly, it binds to damaged DNA with the same affinity with which it binds non-damaged DNA.

Based on its amino acid sequence, Dsup is predicted to be an intrinsically disordered protein. Consistent with this, a recent study also reported a SAXS analyses of Dsup [38]. Our SAXS data is consistent with this recently reported SAXS data on Dsup collected in water, in 2.3 M urea, and in buffer with 2.3 M urea. It differs slightly from the recently reported SAXS data collected in buffer alone, which yielded an R_g equal to 60 Å and D_{max} equal to 200 Å (compared to 78 Å and 290 Å, respectively, calculated from our data). While these values are smaller than the ones we calculated, they are clearly larger than ones expected for a folded, structured protein (25 Å and 80 Å, respectively) [39]. This slight discrepancy between the results reported here and those reported recently is likely due to the prior study using a slightly shorter Dsup construct (lacking the 10-residue FLAG tag), a different buffer (HEPES vs. PBS), and a different computational approach to calculating the R_g and D_{max} values.

Our analyses, however, went significantly further in showing Dsup to be largely disordered. We combined the SAXS data with BD simulations using the full-ensemble method that we previously developed for describing intrinsically disordered proteins. In doing so, we generated an ensemble of 30,000 structures that when combined, agreed well with the experimental SAXS data including the fit of the scattering data (χ^2 is 5.8), the R_g (78 Å), and the D_{max} value (290 Å). Examination of this ensemble showed the Dsup is indeed intrinsically disordered and possesses a high degree of conformational flexibility by sampling a wide range of conformational space.

Based on nuclear localization data, several groups have claimed that the C-terminal region of Dsup (residues 360–445) is both necessary and sufficient for DNA binding [9,10]. Thus, we used BLI to directly test this claim. We found that the C-terminal fragment (residues 355–445) by itself binds DNA with 2,000-fold weaker affinity (K_d is 3 μM) than full-length Dsup binds DNA (K_d is 1.5 nM). This demonstrates that the C-terminal region is not sufficient for high affinity DNA binding. Similarly, we found that the N-terminal fragment (residues 1–355) by itself binds DNA (K_d is 400 nM), albeit with 200-fold lower affinity relative to full-length Dsup. This demonstrates that the C-terminal region is not necessary for DNA binding. Moreover, we generated a set of N-terminal nested deletion mutants of Dsup to better define the regions of Dsup involved in DNA binding. We found that as longer protein

constructs are used, the binding affinity for DNA increases, until full binding affinity was achieved when at least 60% of the protein was present (residues 180–445). These studies suggest that the interactions between Dsup and DNA are multi-valent and involve multiple residues distributed throughout the C-terminal 60% of the protein.

One likely mechanism by which Dsup protects DNA from radiation-induced damage is by altering the conformation of the bound DNA and stabilizing it in a state that is less susceptible to damage. To determine whether the formation of a Dsup-DNA complex alters the conformation of either the Dsup protein or the DNA ligand, we used IR spectroscopy and 2-aminopurine fluorescence. Analyses of the IR spectra revealed conformational shifts in both Dsup and the DNA upon DNA binding. Dsup gains α-helical content suggesting it becomes somewhat more ordered when it binds DNA. This seemingly agrees with a recent study that used circular dichroism to argue that the secondary structure of Dsup, upon binding DNA, shows about 5% change in secondary structure [38]. Addressing which regions of Dsup become more ordered will require further work. Similarly, we showed that the DNA ligand has a reduction in base pairing suggesting partial melting or unwinding of the DNA when Dsup binds. This result was recapitulated using fluorescence spectroscopy and a 2-aminopurine containing DNA substrate. Although the extent of this unwinding is currently unclear, it does suggest that Dsup binding may result in DNA underwinding.

The biochemical and structural studies of Dsup reported here support a general model of DNA protection by Dsup (Figure 12). In this model, Dsup binds with high affinity and potentially coats the DNA. Upon binding, the DNA changes conformation possibly by partial unwinding or underwinding. This could make the formation of the cyclobutane pyrimidine dimers and other photoproducts less efficient by positioning the adjacent bases on the same DNA strand further apart and less susceptible to crosslinking. In addition, Dsup could also employ other strategies to improve resistance to radiation such as acting as a scaffold to bind DNA repair proteins or dehydrating the DNA to reduce damage induced by reactive oxygen species [9,11,12]. While much work remains to be done to decipher the protective mechanism of Dsup, the results reported here are a significant step forward in understanding the biochemical and structural properties of Dsup protein. These findings offer new insights into how disordered proteins such as Dsup can function as radioprotectants in extreme environments.

Supplementary Material

Refer to Web version on PubMed Central for supplementary material.

Acknowledgments

This work was supported by award R35 GM148186 to M.T.W. from the National Institute of General Medical Sciences. The content is solely the responsibility of the authors and does not necessarily reflect the official views of the National Institute of General Medical Sciences or the National Institutes of Health. We thank Maria Spies, Lynne Dieckman, Bret Freudenthal, Christine Kondratick, Zach Frevert, Sarah Jordan, and Luke Handlos for discussions. We thank James Kadonaga at University of California San Diego for the Dsup-expressing plasmid. We thank Wellington Leite at Oak Ridge National Laboratory (Oak Ridge, TN) for collecting small-angle X-ray data. We also thank Richard Huang at RedShiftBio (Boston, MA) for collecting and analyzing the microfluidic modulation spectroscopic data.

DATA AVAILABILITY

Data will be made available on request.

Appendix A. Supplementary material

Supplementary material to this article can be found online at https://doi.org/10.1016/j.jmb.2025.169490.

Abbreviations:

BD	Brownian dynamics
BLI	biolayer interferometry
D_{max}	maximal particle distance
Dsup	damage suppressor
IR	infrared
R_g	radius of gyration
SAXS	small-angle X-ray scattering

References

[1]. Arakawa K, (2022). Examples of extreme survival: tardigrade genomics and molecular anhydrobiology. Annu. Rev. Anim. Biosci. 10, 17–37. [PubMed: 35167318]

[2]. Møbjerg N, Neves RC, (2021). New insights into survival strategies of tardigrades. Comp. Biochem. Physiol. Part A Mol. Integr. Physiol. 254, 110890.

[3]. Nelson DR, (2002). Current status of the tardigrada: evolution and ecology. Integr. Comp. Biol. 42, 652–659. [PubMed: 21708761]

[4]. Horikawa DD, Sakashita T, Katagiri C, Watanabe M, Kikawada T, Nakahara Y, Hamada N, Wada S, Funayama T, Higashi S, Kobayashi Y, Okuda T, Kuwabara M, (2006). Radiation tolerance in the tardigrade *Milnesium tardigradum*. Int. J. Radiat Biol. 82 (12), 843–848. [PubMed: 17178624]

[5]. Jönsson KI, Rabbow E, Schill RO, Harms-Ringdahl M, Rettberg P, (2008). Tardigrades survive exposure to space in low Earth orbit. Curr. Biol. 18 (17), R729–R731. [PubMed: 18786368]

[6]. Hesgrove C, Boothby TC, (2020). The biology of tardigrade disordered proteins in extreme stress tolerance. Cell Commun. Signal 18 (1), 178. [PubMed: 33148259]

[7]. Jönsson KI, (2019). Radiation tolerance in tardigrades: current knowledge and potential applications in medicine. Cancers 11 (9), 1333. [PubMed: 31505739]

[8]. Jönsson KI, Holm I, Tassidis H, (2019). Cell biology of the tardigrades: current knowledge and perspectives. Results Probl. Cell Differ. 68, 231–249. [PubMed: 31598859]

[9]. Hashimoto T, Kunieda T, (2017). DNA protection protein, a novel mechanism of radiation tolerance: lessons from tardigrades. Life (Basel, Switzerland) 7 (2), 26. [PubMed: 28617314]

[10]. Aguilar R, Khan L, Arslanovic N, Birmingham K, Kasliwal K, Posnikoff S, Chakraborty U, Hickman AR, Watson R, Ezell RJ, Willis HE, Cowles MW, Garner R, Shim A, Gutierrez I, Marunde MR, Keogh MC, Tyler JK, (2023). Multivalent binding of the tardigrade Dsup protein to chromatin promotes yeast survival and longevity upon exposure to oxidative damage. Res. Sq.. rs.3.rs-3182883.

[11]. Chavez C, Cruz-Becerra G, Fei J, Kassavetis GA, Kadonaga JT, (2019). The tardigrade damage suppressor protein binds to nucleosomes and protects DNA from hydroxyl radicals. eLife 8, e47682.

[12]. Mínguez-Toral M, Cuevas-Zuviría B, Garrido-Arandia M, Pacios LF, (2020). A computational structural study on the DNA-protecting role of the tardigrade-unique Dsup protein. Sci. Rep. 10 (1), 13424. [PubMed: 32770133]

[13]. Kirke J, Jin XL, Zhang XH, (2020). Expression of a tardigrade Dsup gene enhances genome protection in plants. Mol. Biotechnol. 62 (11–12), 563–571. [PubMed: 32955680]

[14]. Alegrio-Louro J, Cruz-Becerra G, Kadonaga JT, Leschziner AE, (2025). Structural basis of nucleosome recognition by the conserved Dsup and HMGN nucleosome-binding motif. bioRxiv. 2025.01.06.631586.

[15]. Ricci C, Riolo G, Marzocchi C, Brunetti J, Pini A, Cantara S, (2021). The tardigrade damage suppressor protein modulates transcription factor and DNA repair genes in human cells treated with hydroxyl radicals and UV-C. Biology 10 (10), 970. [PubMed: 34681069]

[16]. Young G, Hundt N, Cole D, Fineberg A, Andrecka J, Tyler A, Olerinyova A, Ansari A, Marklund EG, Collier MP, Chandler SA, Tkachenko O, Allen J, Crispin M, Billington N, Takagi Y, Sellers JR, Eichmann C, Selenko P, Frey L, Kukura P, (2018). Quantitative mass imaging of single biological macromolecules. Science (New York, N.Y.) 360 (6387), 423–427. [PubMed: 29700264]

[17]. Hopkins JB, Gillilan RE, Skou S, (2017). BioXTAS RAW: improvements to a free open-source program for small-angle X-ray scattering data reduction and analysis. J. Appl. Cryst. 50 (Pt 5), 1545–1553. [PubMed: 29021737]

[18]. Svergun DI, (1992). Determination of the regularization parameter in indirect-transform methods using perceptual criteria. J. Appl. Cryst. 25, 495–503.

[19]. Abramson J, Adler J, Dunger J, Evans R, Green T, Pritzel A, Ronneberger O, Willmore L, Ballard AJ, Bambrick J, Bodenstein SW, Evans DA, Hung CC, O'Neill M, Reiman D, Tunyasuvunakool K, Wu Z, Žemgulytė A, Arvaniti E, Beattie C, et al. , (2024). Accurate structure prediction of biomolecular interactions with AlphaFold 3. Nature 630 (8016), 493–500. [PubMed: 38718835]

[20]. Powers KT, Gildenberg MS, Washington MT, (2019). Modeling conformationally flexible proteins with X-ray scattering and molecular simulations. Comput. Struct. Biotechnol. J. 17, 570–578. [PubMed: 31073392]

[21]. Powers KT, Elcock AH, Washington MT, (2018). The C-terminal region of translesion synthesis DNA polymerase g is partially unstructured and has high conformational flexibility. Nucleic Acids Res. 46 (4), 2107–2120. [PubMed: 29385534]

[22]. Gildenberg MS, Washington MT, (2019). Conformational flexibility of fork-remodeling helicase Rad5 shown by full-ensemble hybrid methods. PLoS One 14, (10)e0223875

[23]. Frembgen-Kesner T, Elcock AH, (2010). Absolute protein-protein association rate constants from flexible, coarse-grained Brownian dynamics simulations: the role of intermolecular hydrodynamic interactions in Barnase-Barstar association. Biophys. J. 99 (9), L75–L77. [PubMed: 21044566]

[24]. Elcock AH, (2006). Molecular simulations of cotranslational protein folding: fragment stabilities, folding cooperativity, and trapping in the ribosome. PLoS Comput. Biol. 2 (7), e98. [PubMed: 16789821]

[25]. Frembgen-Kesner T, Elcock AH, (2009). Striking effects of hydrodynamic interactions on the simulated diffusion and folding of proteins. J. Chem. Theory Comput. 5 (2), 242–256. [PubMed: 26610102]

[26]. Ripley BM, Reusch DT, Washington MT, (2020). Yeast DNA polymerase g possesses two PIP-like motifs that bind PCNA and Rad6-Rad18 with different specificities. DNA Repair 95, 102968.

[27]. Lucas L, Tsoi PS, Nair A, Ferreon ACM, Ferreon JC, (2025). Sensing protein structural transitions with microfluidic modulation infrared spectroscopy. Biosensors 15 (6), 382. [PubMed: 40558464]

[28]. Wei B, Ma E, Tang S, Cadang L, Collins V, Gorman S, Chen B, Huang R, Wang J, Ma M, Zhang K, (2025). Real-time monitoring of higher-order structure of RNAs by temperature-course size exclusion chromatography and microfluidic modulation spectroscopy. Anal. Chem. 97 (10), 5632–5642. [PubMed: 40014844]

[29]. Barth A, Zscherp C, (2002). What vibrations tell us about proteins. Q. Rev. Biophys. 35 (4), 369–430. [PubMed: 12621861]

[30]. Reppert M, Tokmakoff A, (2016). Computational amide I 2D IR spectroscopy as a probe of protein structure and dynamics. Annu. Rev. Phys. Chem. 67, 359–386. [PubMed: 27023758]

[31]. Krummel AT, Zanni MT, (2006). DNA vibrational coupling revealed with two-dimensional infrared spectroscopy: insight into why vibrational spectroscopy is sensitive to DNA structure. J. Phys. Chem. B 110 (28), 13991–14000. [PubMed: 16836352]

[32]. Jiang Y, Wang L, (2020). Modeling the vibrational couplings of nucleobases. J. Chem. Phys. 152, (8)084114

[33]. Jean JM, Hall KB, (2001). 2-Aminopurine fluorescence quenching and lifetimes: role of base stacking. PNAS 98 (1), 37–41. [PubMed: 11120885]

[34]. Rachofsky EL, Osman R, Ross JB, (2001). Probing structure and dynamics of DNA with 2-aminopurine: effects of local environment on fluorescence. Biochemistry 40 (4), 946–956. [PubMed: 11170416]

[35]. Jones AC, Neely RK, (2015). 2-Aminopurine as a fluorescent probe of DNA conformation and the DNA-enzyme interface. Q. Rev. Biophys. 48 (2), 244–279. [PubMed: 25881643]

[36]. Crowe JH, (2015). Anhydrobiosis: an unsolved problem with applications in human welfare. Subcell. Biochem. 71, 263–280. [PubMed: 26438269]

[37]. Wright JC, (1989). Desiccation tolerance and water-retentive mechanisms in tardigrades. J. Exp. Biol. 142 (1), 267–292.

[38]. Zarubin M, Murugova T, Ryzhykau Y, Ivankov O, Uversky VN, Kravchenko E, (2024). Structural study of the intrinsically disordered tardigrade damage suppressor protein (Dsup) and its complex with DNA. Sci. Rep. 14 (1), 22910. [PubMed: 39358423]

[39]. Putnam CD, Hammel M, Hura GL, Tainer JA, (2007). X-ray solution scattering (SAXS) combined with crystallography and computation: defining accurate macromolecular structures, conformations and assemblies in solution. Q. Rev. Biophys. 40 (3), 191–285. [PubMed: 18078545]

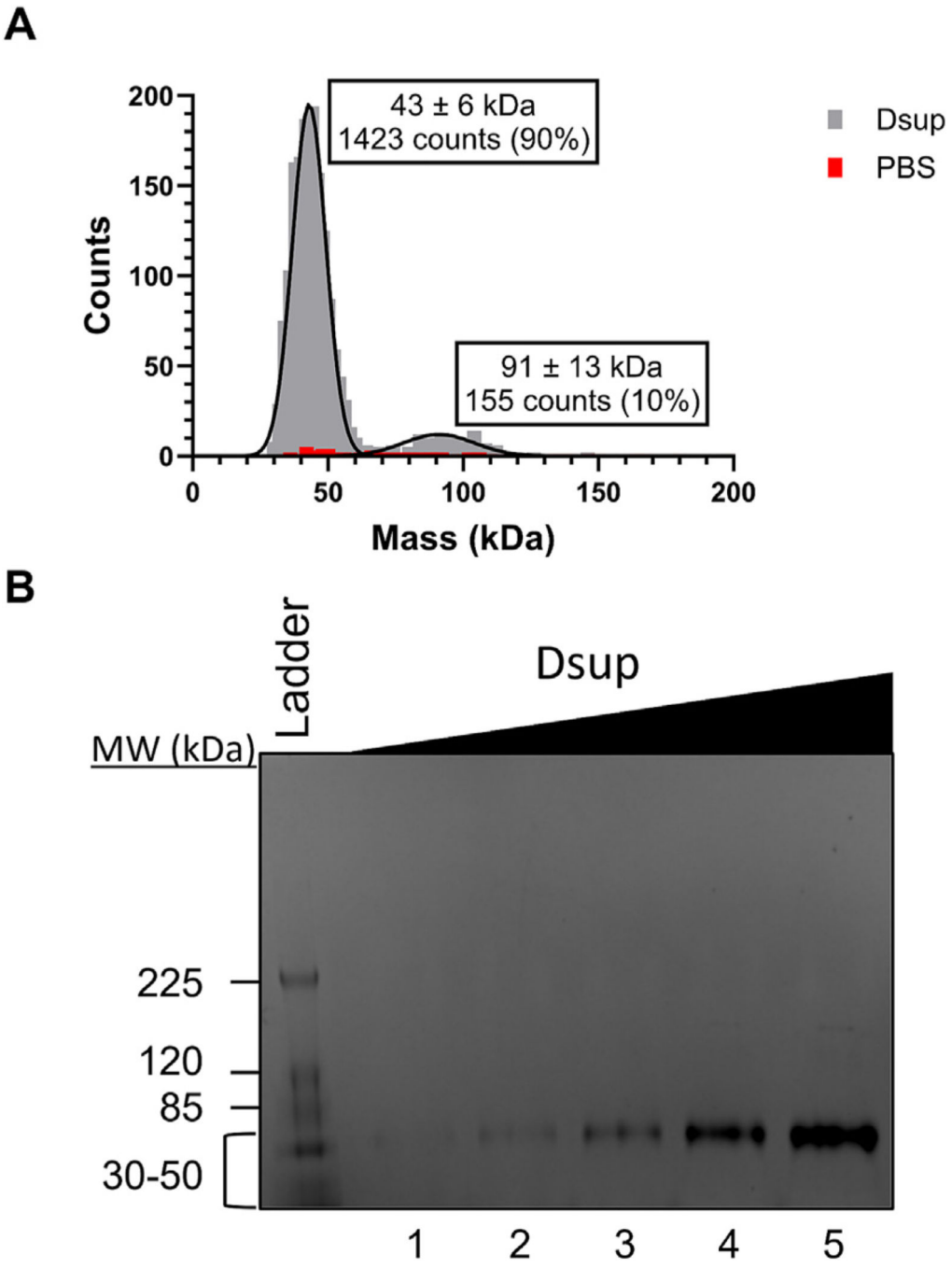

Figure 1. Mass photometry analyses of Dsup.

(**A**) Purified Dsup (20 nM) was subjected to mass photometry. The grey histogram shows that the majority of the protein (90%) was 43 kDa (which corresponds to a monomer), while a minority (10%) was 91 kDa (which corresponds to a dimer). The red histogram represents a control experiment using buffer alone (*i.e.*, in the absence of Dsup). (**B**) Blue native PAGE showing the oligomeric state of Dsup at 0.1, 0.2, 0.5, 1, 2 μM final concentrations. At all of these concentrations, we observe only a single band corresponding to approximately 40–50 kDa.

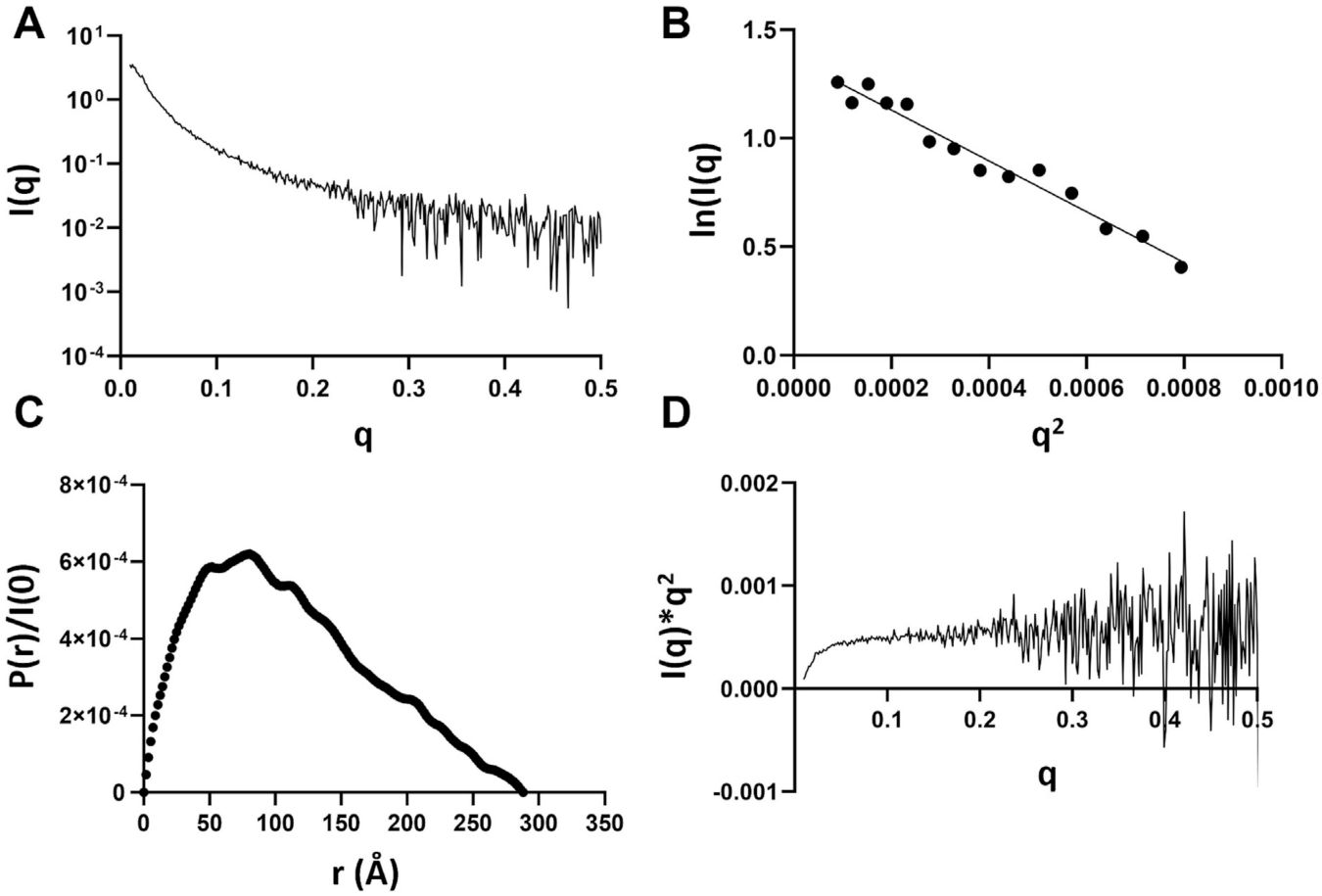

Figure 2. Small-angle X-ray scattering of Dsup.

(**A**) The X-ray scattering curve of purified Dsup is shown. (**B**) The Guinier plot is linear (R^2 = 0.97) showing no significant aggregation. (**C**) The pairwise distance distribution function, $P(r)$, curve reveals a radius of gyration (R_g) of 78 Å and a maximum particle dimension (D_{max}) of 290 Å. (**D**) The Kratky plot shows a lack of structure for purified Dsup.

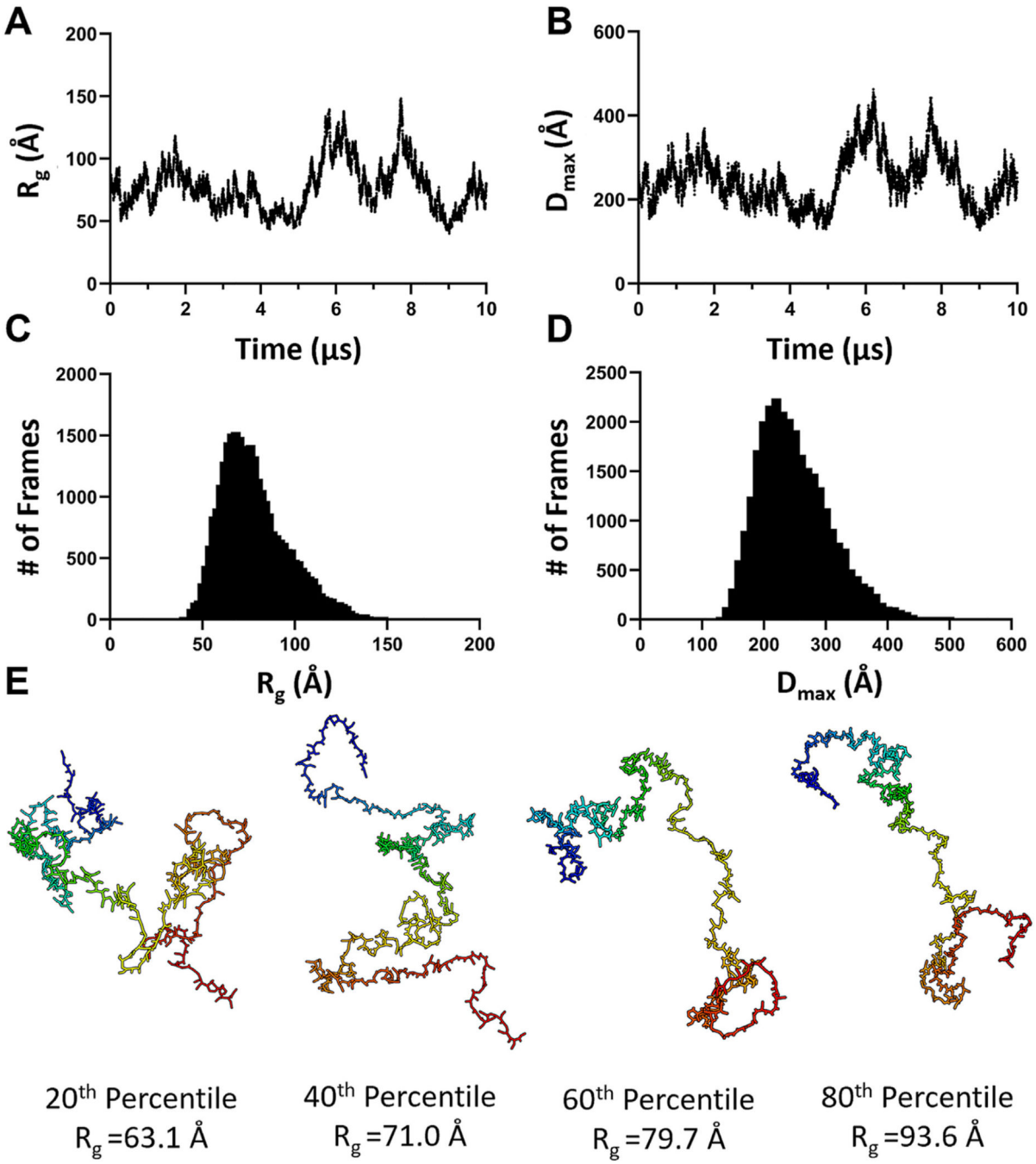

Figure 3. Brownian dynamics simulations of Dsup.

(**A**) A representative plot of the radius of gyration (R_g) as a function of simulation time for one replicate. (**B**) A representative plot of the maximum particle dimension (D_{max}) as a function of simulation time for one replicate. (**C**) The histogram shows the distribution of R_g values for all replicates combined. The average R_g value for all replicates is 78 Å, which equals to the experimental value obtained from SAXS. (**D**) The histogram shows the distribution of D_{max} values for all replicates combined. The experimental value obtained from SAXS (290 Å) occurs at the 75th percentile in the D_{max} distribution. (**E**)

Individual structures of Dsup from the simulations representing the 20th, 40th, 60th, and 80th percentiles of R_g distribution with the N-termini shown in *blue* and the C-termini shown in *red*.

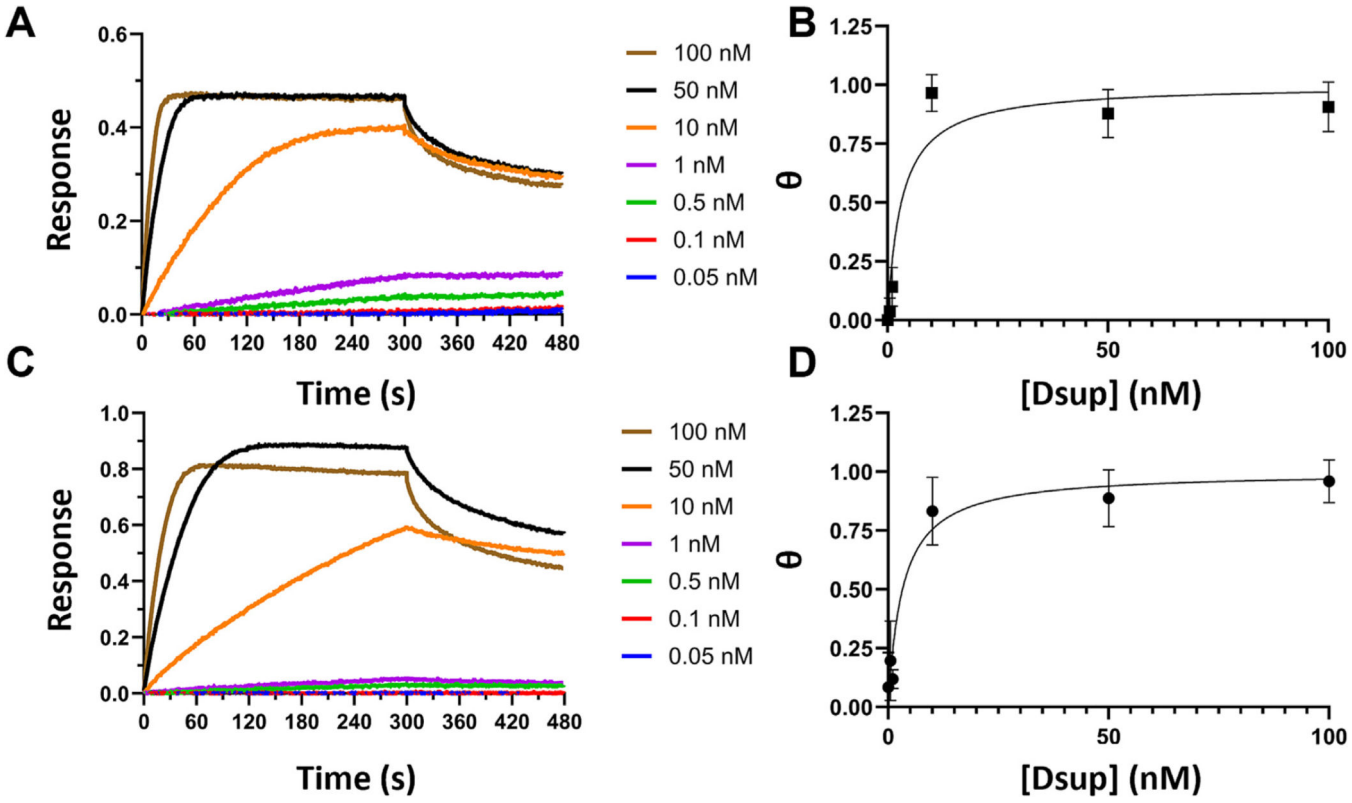

Figure 4. Single-stranded and double-stranded DNA binding by Dsup.

(**A**) The plot shows the BLI response units as a function of time for the association (1–300 s) and dissociation (300–480 s) phases for an immobilized 30-mer double-stranded DNA binding to various concentrations of Dsup. (**B**) The plot shows the normalized equilibrium response units as a function of Dsup concentration for a 30-mer double-stranded DNA ligand. The affinity between Dsup and the double-stranded DNA is 3.1 ± 0.7 nM. (**C**) The plot shows the of biolayer interferometry (BLI) response units as a function of time for the association (1–300 s) and dissociation (300–480 s) phases for an immobilized 30-mer double-stranded DNA binding to various concentrations of purified Dsup. (**D**) The plot shows the normalized equilibrium response units as a function of Dsup concentration for a 30-mer single-stranded DNA ligand. The affinity between Dsup and the single-stranded DNA is 3.2 ± 0.8 nM.

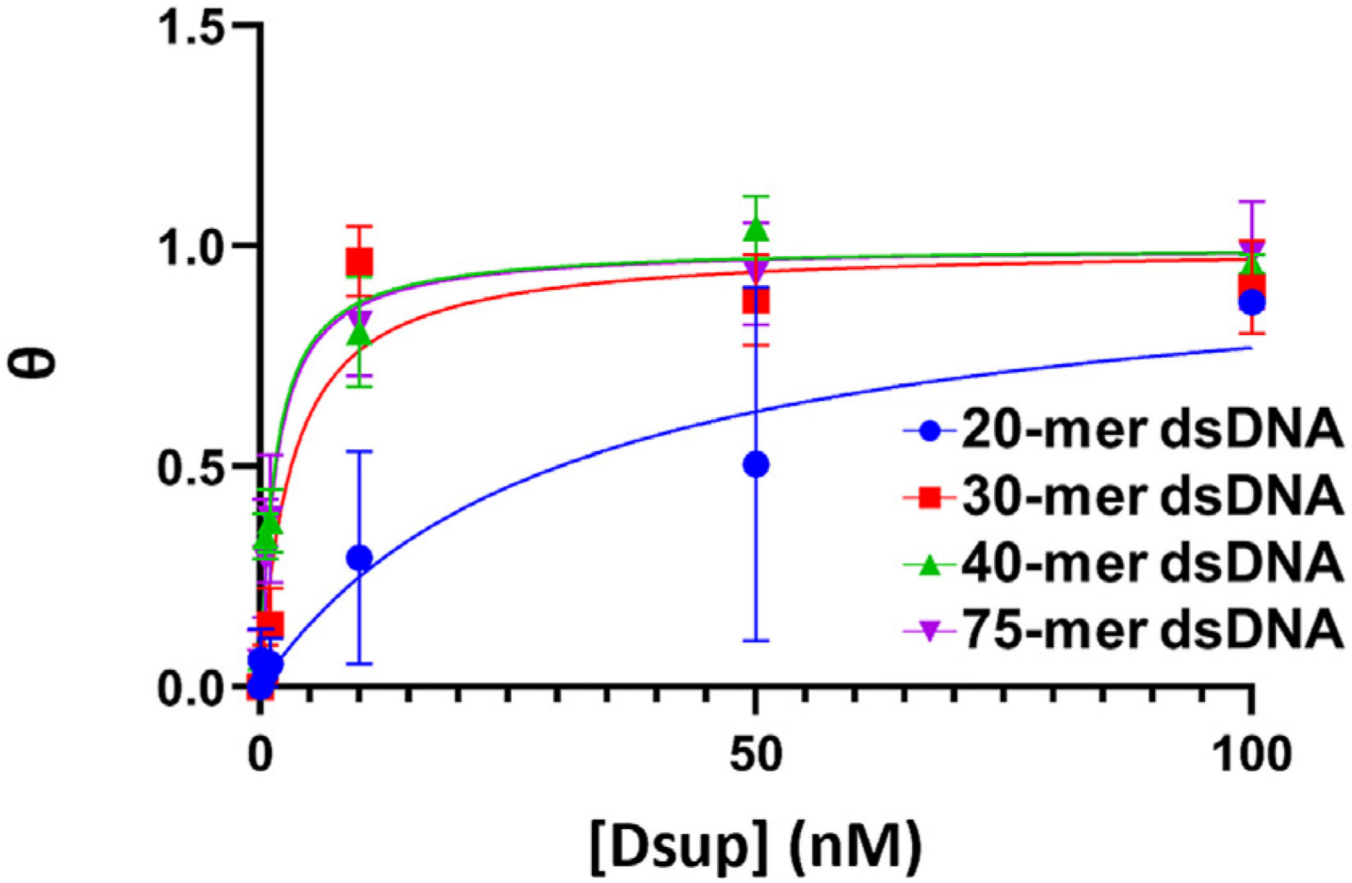

Figure 5. DNA length for optimal DNA-binding by Dsup.

The plot shows the normalized equilibrium BLI response units as a function of Dsup concentration for a 20-mer double-stranded DNA (*blue*), 30-mer double-stranded DNA (*red*), 40-mer double-stranded DNA (*green*), and a 75-mer double-stranded DNA (*purple*). The K_d values for each of these DNA ligands are listed in Table 1.

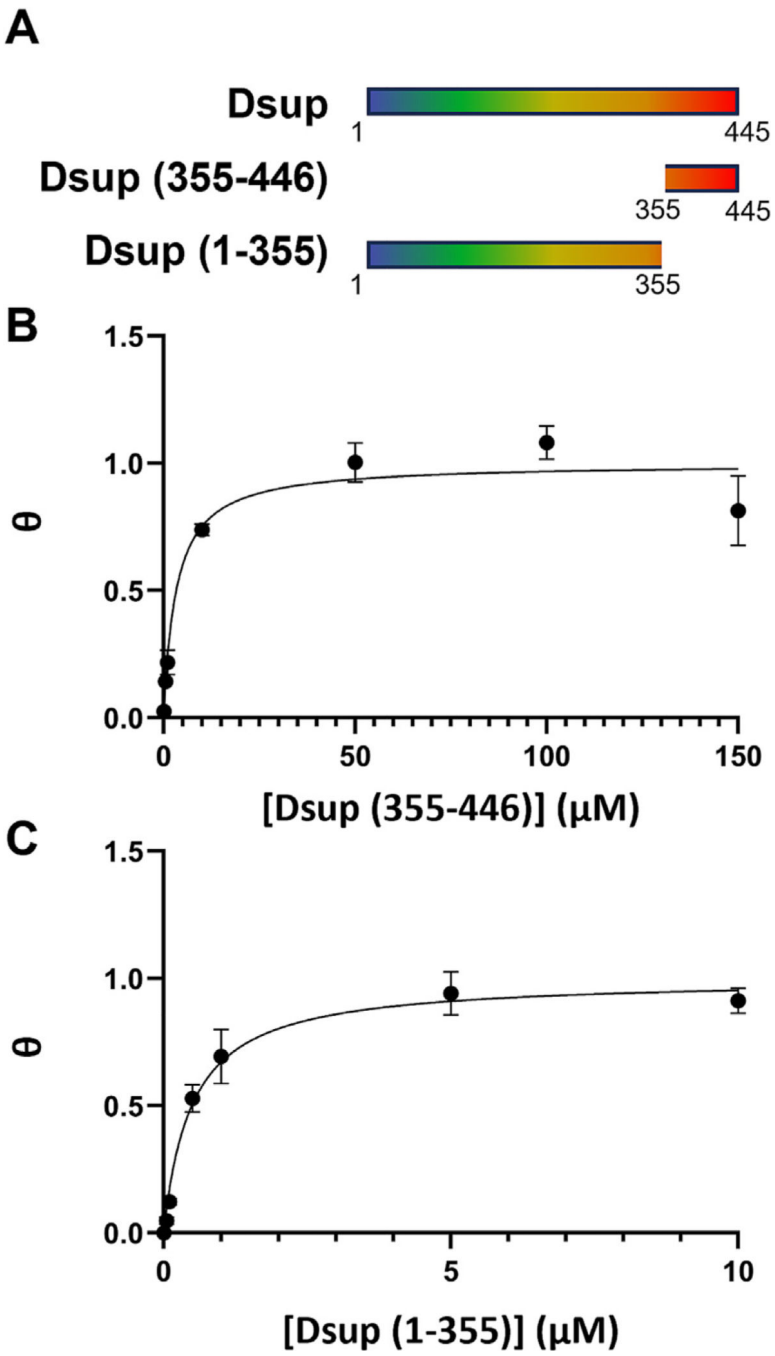

Figure 6. DNA binding by the N-terminal and C-terminal regions of Dsup.

(**A**) Diagram showing full-length Dsup as well as the C-terminal region of Dsup (residues 335–445) and the N-terminal region of Dsup (residues 1–355). (**B**) The plot shows the normalized equilibrium BLI response units as a function of Dsup concentration for a 40-mer double-stranded DNA ligand and the C-terminal region of Dsup. The K_d for C-terminal region of Dsup binding DNA is 3.3 ± 0.6 μM. (**C**) The plot shows the normalized equilibrium response units as a function of Dsup concentration for a 40-mer double-stranded

DNA ligand and the N-terminal region of Dsup. The K_d for N-terminal region of Dsup binding DNA is 0.49 ± 0.4 μM.

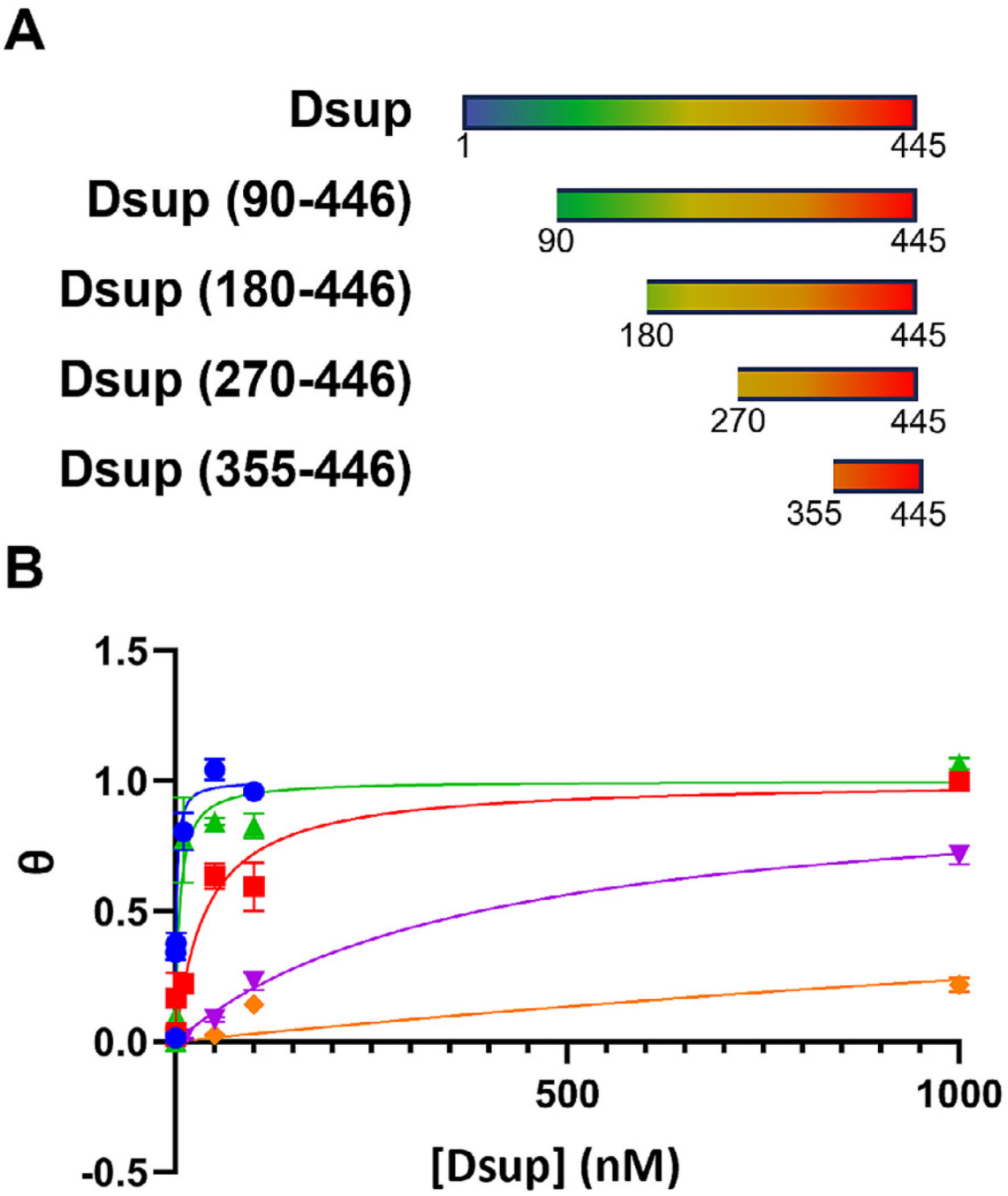

Figure 7. DNA binding by truncated Dsup proteins.

(**A**) Diagram showing full-length Dsup as well as the various truncated constructs of Dsup (residues 90–445, 180–445, 270–445, and 355–445). (**B**) The plot shows the normalized equilibrium BLI response units as a function of Dsup concentration for a 40-mer double-stranded DNA for various truncated constructs of Dsup: full-length Dsup (*blue*), Dsup (residues 90–445) (*red*), Dsup (residues 180–445) (*green*), Dsup (residues 355–445) (*purple*), and Dsup (residues 270–445) (*orange*). The K_d values for each of these Dsup constructs are listed in Table 2.

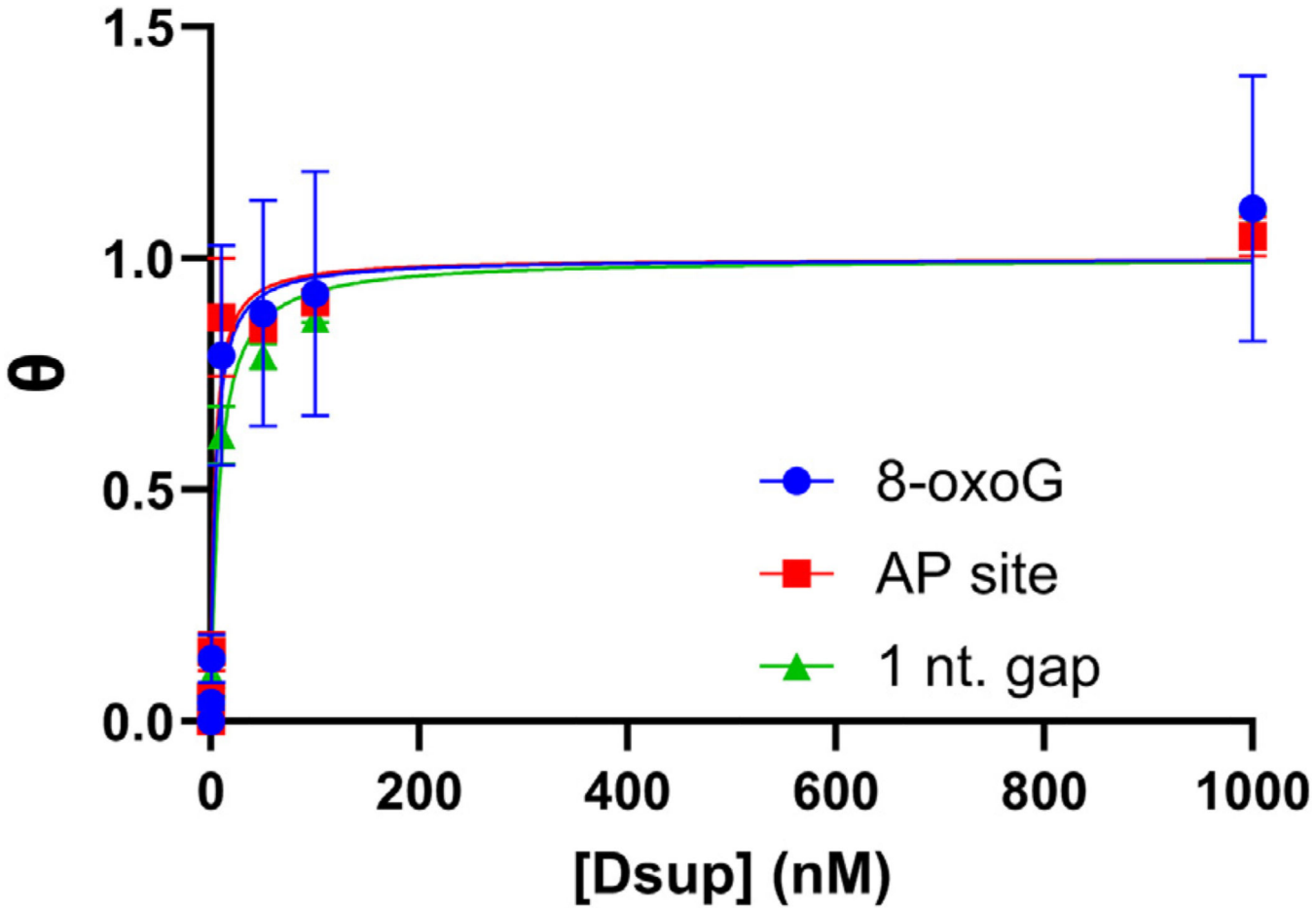

Figure 8. Damaged DNA binding by Dsup.

The plot shows the normalized equilibrium BLI response units as a function of Dsup concentration for a 40-mer double-stranded DNA containing a single 8-oxoguanine lesion (*blue*), a single abasic site (*red*) and a single 1-nucleotide gap (*green*). The K_d values for each of these DNA molecules are listed in Table 3.

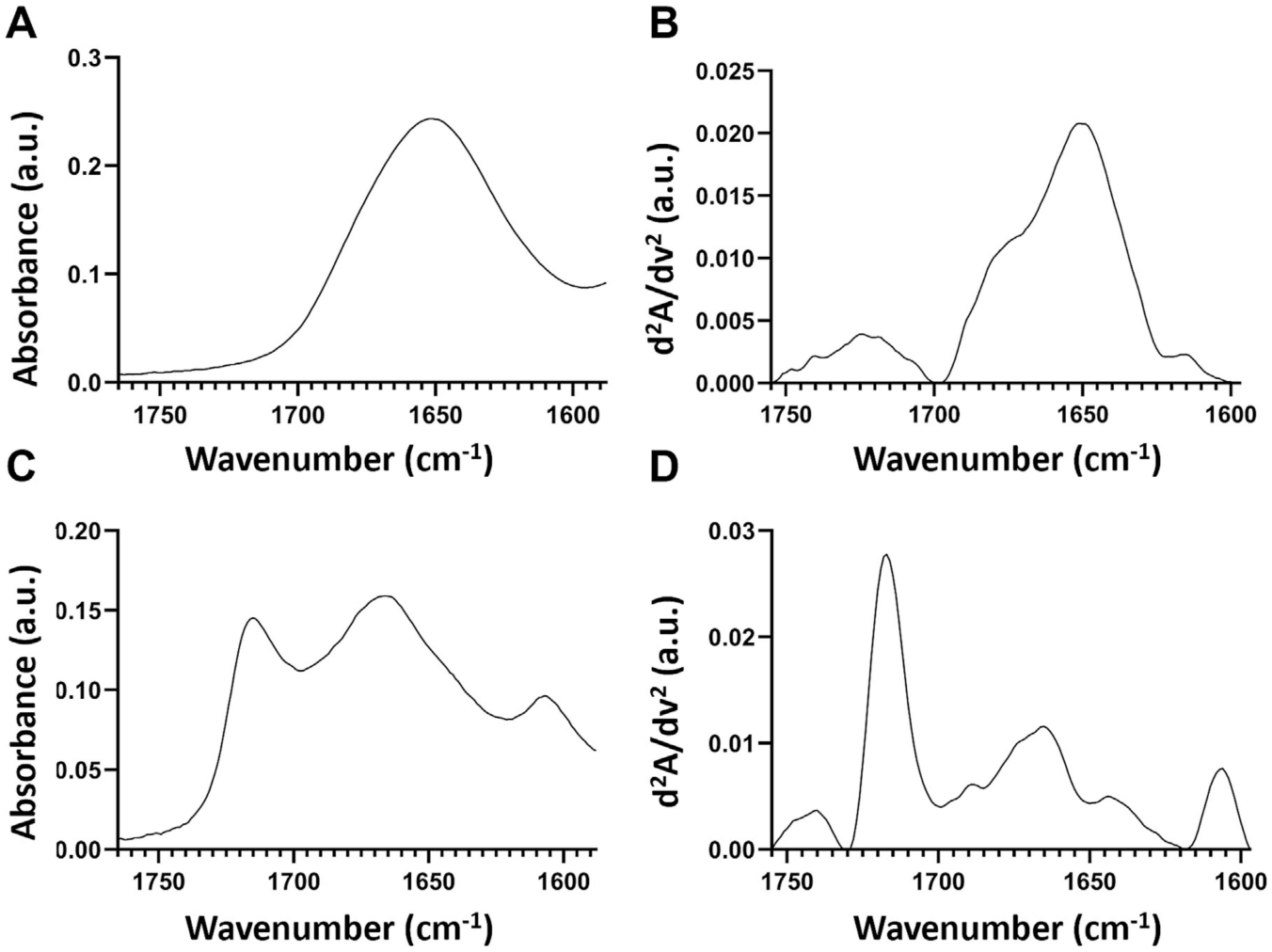

Figure 9. Microfluidic modulation spectroscopy of Dsup and DNA alone.

(**A**) The plot shows the buffer-subtracted absorbance averaged over three replicates graphed as a function of wavenumber in the amide I bond region for purified Dsup. (**B**) The inverse second derivative of the spectral data for purified Dsup is shown. (**C**) The plot shows the buffer-subtracted absorbance averaged over three replicates graphed as a function of wavenumber in the amide I bond region for the 40-mer DNA ligand. (**D**) The inverse second derivative of the spectral data for purified Dsup is shown.

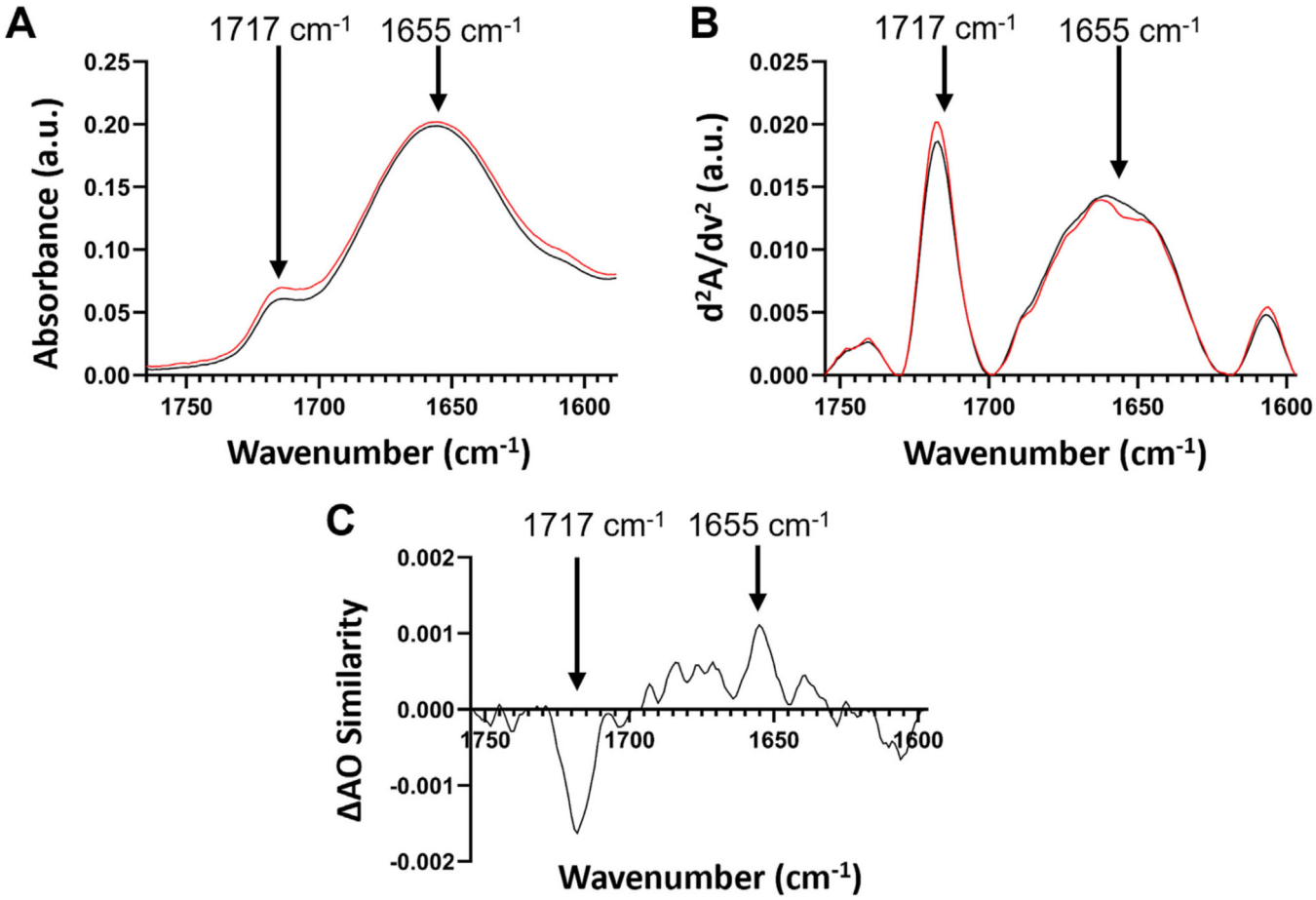

Figure 10. Microfluidic modulation spectroscopy of the Dsup-DNA complex.

(**A**) The plot shows the buffer-subtracted absorbance averaged over three replicates graphed as a function of wavenumber in the amide I bond region for Dsup-DNA complex (*black*). The plot of the theoretical absorbance of the complex assuming no conformational changes in either the protein or DNA upon complex formation is shown (*red*). (**B**) The inverse second derivative plot of the experimental data for the Dsup-DNA complex as a function of wavenumber is shown (*black*), and the inverse second derivative plot of the theoretical data for this complex is shown (*red*). (**C**) The plot shows the differences between the experimental and theoretical spectra for the Dsup-DNA complex as a function of wavenumber. A loss of signal at 1717 cm^{-1} indicates reduced base pairing in the DNA within the complex, while an increase at 1655 cm^{-1} indicates the existence of more α-helical content in Dsup within the complex.

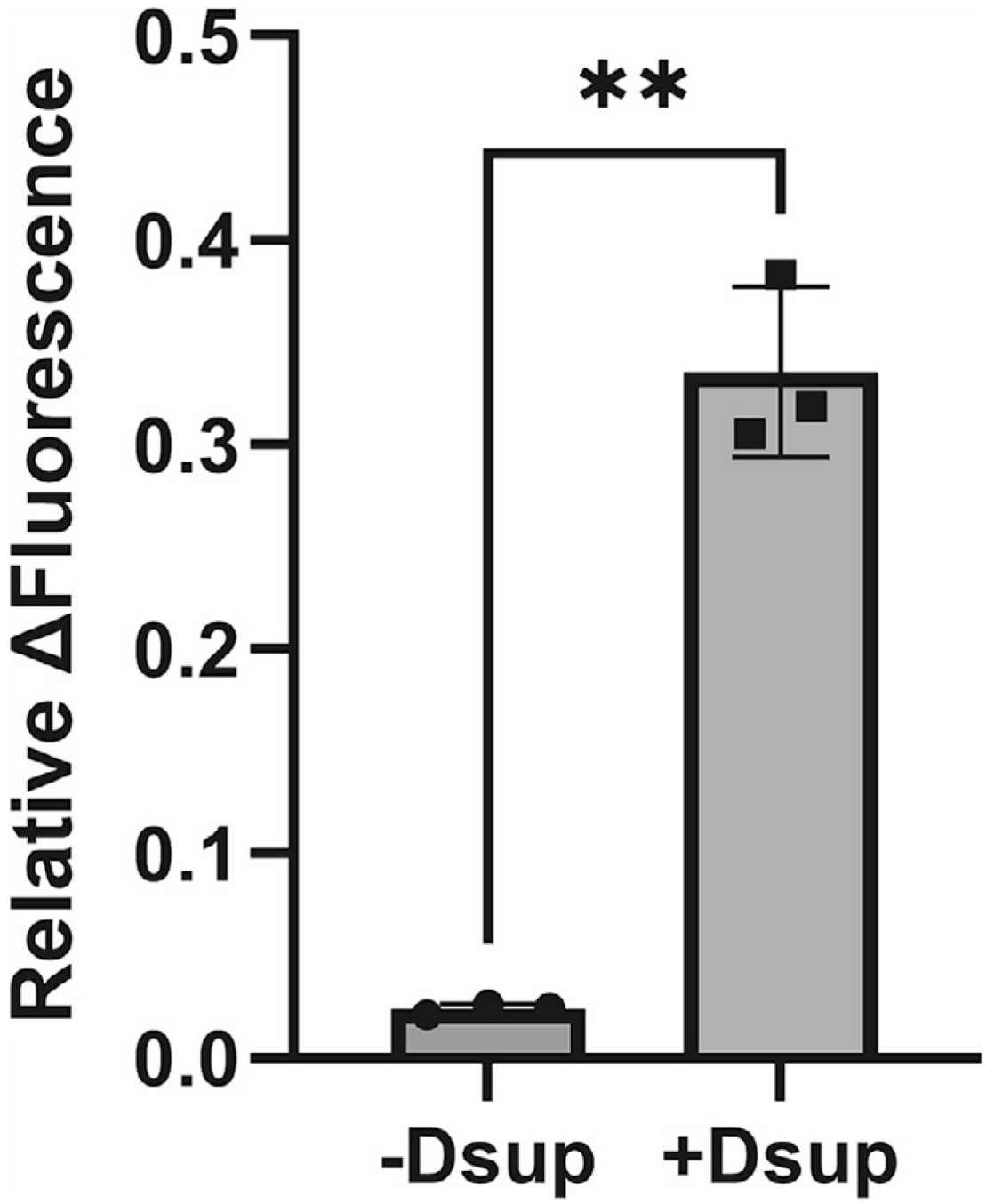

Figure 11. Dsup binding to 2-aminopurine-containing DNA.

The histogram shows the normalized and background-subtracted fluorescence reading (in arbitrary units) for a 30-mer DNA molecule (1 nM) containing two 2-aminopurines in the presence or absence of 4 nM Dsup. The fluorescence increase upon Dsup binding indicates the partial melting or unwinding of the DNA duplex.

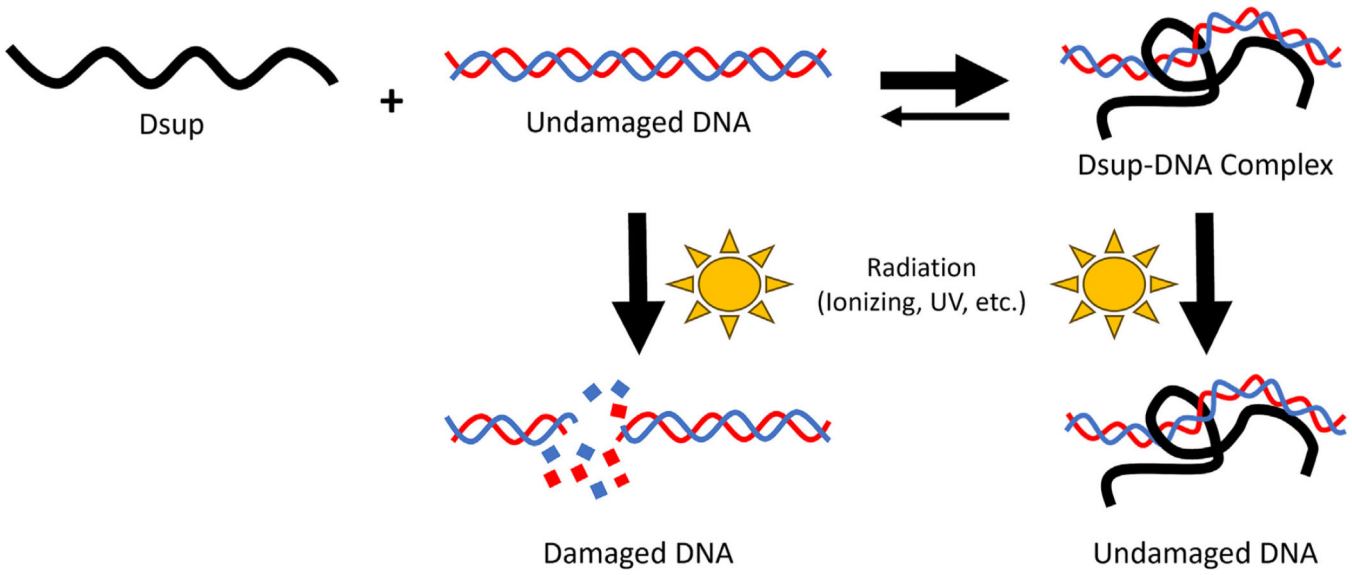

Figure 12. General mechanism of DNA protection by Dsup.

Dsup binds undamaged DNA and both Dsup and the DNA undergo conformational changes upon complex formation. The conformation of the DNA in bound to Dsup is less susceptible to radiation-induced damage than the DNA not bound to Dsup.

Table 1

DNA length for optimal DNA-binding by Dsup.

	K_d (nM)	ΔG (kJ/mol)
20-mer DNA	30 ± 8	−43 ± 1
30-mer DNA	3.1 ± 0.7	−49 ± 1
40-mer DNA	1.5 ± 0.2	−50 ± 1
75-mer DNA	1.6 ± 0.2	−50 ± 1

Table 2

DNA binding by truncated Dsup proteins.

	K_d (nM)	ΔG (kJ/mol)
Dsup (1–445)	1.5 ± 0.2	−50 ± 1
Dsup (90–445)	39 ± 7	−42 ± 1
Dsup (180–445)	5.2 ± 1.4	−47 ± 1
Dsup (270–445)	390 ± 30	−37 ± 1
Dsup (355–445)	3,300 ± 600	−31 ± 1

Table 3

Damaged DNA binding by Dsup.

	K_d (nM)	ΔG (kJ/mol)
8-oxoG	4.3 ± 1.5	−48 ± 1
Abasic site	3.6 ± 0.6	−48 ± 1
1 nt. gap	7.8 ± 0.9	−46 ± 1